Received 30 October 2023; accepted 26 November 2023. Date of publication 30 November 2023; date of current version 19 December 2023.
The review of this article was arranged by Editor G. I. Ng.

Digital Object Identifier 10.1109/JEDS.2023.3337780

Noise Performance Investigation of AlGaN/GaN HEMT With Tall Gate Stem for Millimeter-Wave LNA Application

PING-HSUN LEE [1], YUEH-CHIN LIN [2], HENG-TUNG HSU [3] (Senior Member, IEEE), CHENG-HSIEN YU [2], YI-FAN TSAO [3] (Member, IEEE), PIN SU [1] (Member, IEEE), AND EDWARD YI CHANG [2,3,4] (Life Fellow, IEEE)

1 Institute of Electronics, National Yang Ming Chiao Tung University, Hsinchu 30010, Taiwan
2 Department of Materials Science and Engineering, National Yang Ming Chiao Tung University, Hsinchu 30010, Taiwan
3 International College of Semiconductor Technology, National Yang Ming Chiao Tung University, Hsinchu 30010, Taiwan
4 Department of Electronics Engineering, National Yang Ming Chiao Tung University, Hsinchu 30010, Taiwan

CORRESPONDING AUTHOR: E. Y. CHANG (e-mail: edc@mail.nctu.edu.tw)

This work was supported in part by the "Center for the Semiconductor Technology Research" from the Featured Areas Research Center Program within the Framework of the Higher Education Sprout Project by the Ministry of Education (MOE), Taiwan, and in part by the Ministry of Science and Technology, Taiwan, under Grant NSTC 111-2218-E-A49-021, Grant NSTC 111-2634-F-A49-008, Grant NSTC 111-2221-E-A49-173-MY3, and Grant NSTC 112-2622-8-A49-013–SB.

ABSTRACT In this research, Γ-gated AlGaN/GaN HEMTs with different layout designs and heights of gate stems were fabricated to investigate their impacts on the noise performance in the Ka-band. First, devices with 4 types of gate peripheries were prepared to optimize the layout structure for best noise performance since the values of parasitic capacitance and resistance, which are detrimental to the noise characteristic, vary as the gate widths and the number of fingers change. The device with gate width of 4×50 um achieved the optimal noise performance, minimum noise figure (NF_{min}) of 1.5 dB and associated gain of 6.2 dB at 28 GHz. Next, devices with different gate stem heights were fabricated following the 4×50um layout pattern. The raised gate structure was applied to reduce the parasitic capacitance of the device for RF power performance enhancement, but a taller gate stem unfortunately results in the increment of gate resistance. Therefore, the impact of stem height on NF_{min} remains unknown. According to the experiment results, the device with a stem height of 200 nm stands out to be a viable compromise for the noise and output power performance in the Ka-band, thus providing a positive outlook for the feasibilities of single-chip circuit integration of both LNA and PA at millimeter-wave spectrum.

INDEX TERMS AlGaN/GaN HEMT, noise figure, LNA.

I. INTRODUCTION

The fifth-generation (5G) wireless communication technology exploits millimeter-wave semiconductor devices to meet the demands of rapid and massive data transmission. Transceiver is a critical component of such systems required to sustain high power and low-noise operations at higher frequencies. Low-noise amplifiers (LNA) made of high electron mobility transistors (HEMTs) are often placed in the front end of a transceiver circuit to take advantage of the nature of a 2-dimensional electron gas (2DEG) inherent to HEMT.

GaAs-based LNA device technology has come a long way to reach its current maturity for radio-frequency monolithic-microwave-integrated-circuit (MMIC) applications [1], [2], [3], [4], [5]. However, because of its relatively narrow bandgap of 1.42eV, GaAs cannot sustain high input power in some needs. It's therefore often necessary to insert an off-chip limiter upfront to avoid overloading or damaging, albeit at the sacrifice of added complexities of circuit designs and raising the cost to produce it.

GaN-HEMT based LNAs, by contrast, can endure much higher operational voltages or powers without breakdown.

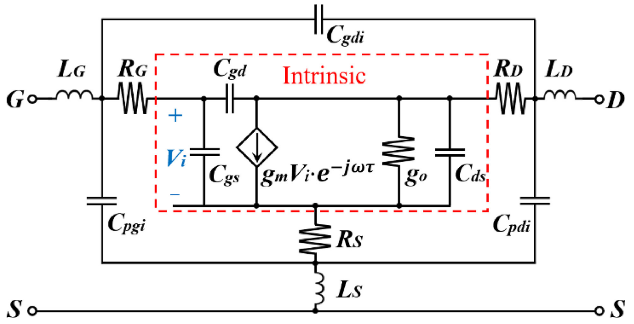

FIGURE 1. **Small-signal equivalent circuit model of the AlGaN/GaN HEMTs in this study.**

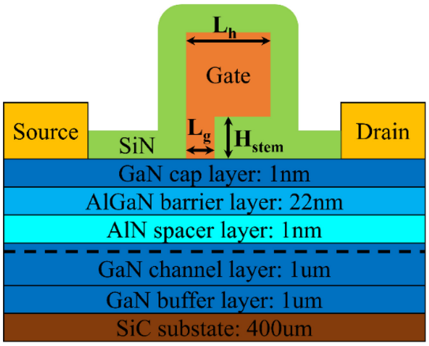

FIGURE 2. **Device structure and epitaxial composition of the Γ-gate AlGaN/GaN HEMTs in this study.**

GaN comes with a wider bandgap of 3.4 eV, higher saturation electron drift velocity and higher electron mobility compared to GaAs under large electric bias. These basic traits make GaN-HEMT superior to GaAs in their abilities to meet millimeter-wave LNA and PA circuit integration (MMIC) needs [6], [7], [8], [9], [10]. Moreover, the noise figures of the GaN-HEMT MMICs continue to get better and have started to catch up with their GaAs counterparts [11], [12], [13], [14], [15], now reported to have reached as low as 1 dB at 37 GHz [16].

This work falls in this category of efforts in seeking technological advances. More specifically, we have fabricated, characterized, and modelled AlGaN/GaN HEMTs of various gate peripheries and heights of gate stems. The objective was to exploit the geometric variations according to how their parasitic capacitance and resistance change to make the noise figures and output power performance better in the Ka-band. Based on an established small-signal equivalent circuit model, elements like the capacitance, resistance, intrinsic transconductance and output conductance can be extracted using the cold-FET method to explain the trends of noise figures [17]. The low- noise performances with comparable power levels serve as a guide to design AlGaN/GaN HEMT devices for possibilities, in particular, of single-chip RF circuit integration of both LNA and PA at millimeter-wave spectrum.

II. EXPERIMENT DESIGN

The noise behaviors of a HEMT are gauged by its minimum noise figure (NF_{min}), noise equivalent resistance (R_n), and optimal source reflection coefficient (Γ_{opt}) of the device as some figures of merits. A designer can simply apply the Fukui equation to estimate the relevant NF_{min} with an established small-signal equivalent circuit model [18]. The small-signal equivalent model of AlGaN/GaN HEMTs in this study is shown in Fig. 1. Where C_{gs}, C_{gd}, and C_{ds} are the intrinsic capacitances, g_m and g_o stand for the intrinsic transconductance and the output conductance, R_G, R_D, R_S are the bias independent resistances, L_G, L_D, L_S are the inductances, and C_{pgi}, C_{pdi}, C_{gdi} stand for the inter-electrode and crossover capacitance between the gate, source, and drain. If having the feed-back capacitance (C_{gd}) taken into account at high frequencies, the Fukui equation can have NF_{min} expressed as

$$NF_{min} = 1 + 2\pi K_f f\left(C_{gs} + C_{gd}\right)\sqrt{\frac{R_G + R_S}{g_m}} \tag{1}$$

where f is the operating frequency and K_f is the Fukui coefficient, which is an empirical number that largely remains constant for those HEMTs of similar epitaxial structures and layout profiles [19], [20]. Based on Equations (1), NF_{min} can be improved by reducing the parasitic resistances and capacitances. Recently, Andrei et al., Roy et al., and Gao et al. have investigated the influence of varying gate periphery on the noise figure of HEMTs [21], [22], [23]; however, the impact of varying the gate periphery on the large-signal power performance, which is quite important as well, has not been discussed. We have recently reported on the AlGaN/GaN HEMT with a properly raised gate stem has lower capacitance (C_{gs} and C_{gd}) values, better f_T and f_{max}, and improved power performance [24]. As a follow on, in this study, at first, AlGaN/GaN HEMTs with different gate peripheries were fabricated to investigate the change in parasitic capacitance and resistance and to optimize gate periphery for best noise performance. The large-signal power performance at 28 GHz of different devices were compared with each other as well. Next, devices with the optimal gate periphery, for both noise and power consideration, were used to investigate the impact of varying gate stem height on the noise performance.

The device structure and the epitaxial layers of the Γ-gate AlGaN/GaN HEMTs in this study are shown in Fig. 2. The Γ-shaped gate was formed with a gate length (L_g) of 150 nm and a head length (L_h) of 350 nm, while the source-drain spacing (L_{SD}) is 2 um. From top to bottom, the epitaxial composition contains the GaN cap layer, AlGaN barrier layer, AlN spacer layer, GaN channel layer, GaN buffer layer, and SiC substrate.

In the first set of experiments, AlGaN/GaN HEMTs with 4 different types of gate peripheries were designed. As shown in Fig. 3 and 4, the gate widths of the devices are 2×25 um, 4×25 um, 2×50 um, and 4×50 um, all with a gate stem height (H_{stem}) of 150 nm. For devices with 4 fingers, the

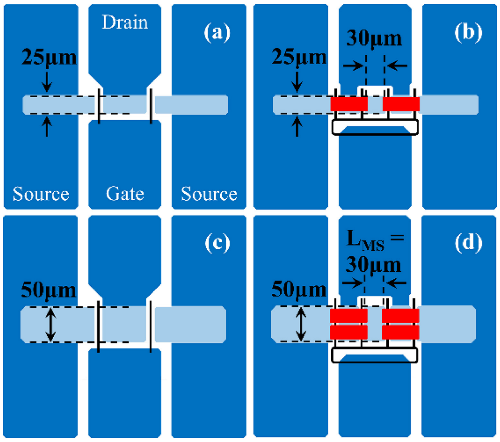

FIGURE 3. **Layout designs of AlGaN/GaN HEMTs with gate widths of (a) 2×25 um (b) 4×25 um (c) 2×50 um (d) 4×50 um in this study.**

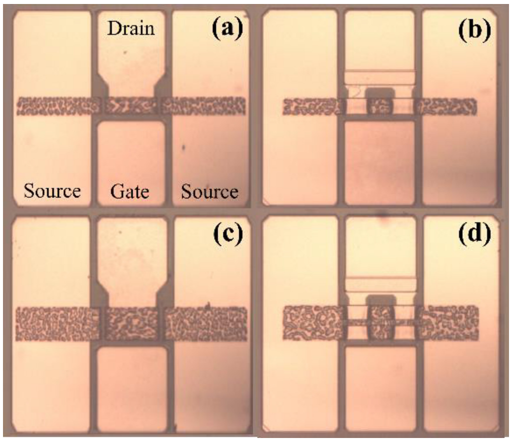

FIGURE 4. **Top view images of AlGaN/GaN HEMTs with gate widths of (a) 2×25 um (b) 4×25 um (c) 2×50 um (d) 4×50 um in this study.**

air-bridge structures are used to connect the source pads and are highlighted as the red area in Fig. 3; on the other hand, the length of the middle source pad (L_{MS}) for 4-finger devices is 30 um.

In the second set of experiments, the AlGaN/GaN HEMTs were fabricated with different gate stem heights of 150, 200, and 250 nm, and their layouts follow the 4×50μm pattern shown in Fig. 3(d).

To characterize the noise and RF large-signal power performance, the devices were measured by Auriga noise parameter measurement system from 18 to 40 GHz and by the load-pull measurement system at 28 GHz. To further understand the characteristics of the parasitic capacitance and resistance, the cold-FET method was applied to extract their values based on the results of S-parameters using a small-signal equivalent circuit model shown in Fig. 1.

III. DEVICE FABRICATION

The fabrication process for AlGaN/GaN HEMTs in this study is similar to the process reported in reference [24]. The fabrication started with Ohmic contact formation. The Ohmic metal of Ti/Al/Ni/Au (20/120/25/100 nm) was deposited by E-gun evaporator and then was annealed in N_2 ambient at 835 °C by RTA. Boron implantation then followed to achieve device isolation. Before the gate formation, the first SiN film was deposited by PECVD and its thickness was used to determine the height of gate stem. Then, the gate shift technology was performed by the stepper photolithography system to form a Γ-shaped gate with a gate length of 150 nm. The gate metal of Ni/Au (50/500 nm) was deposited by E-gun evaporator. The film thinning step used in [24] was adopted in this work as well. The via hole opening was then performed by ICP-RIE. In the end, the deposition of thick Au was conducted for the metallization and the air-bridge structures were fabricated for the 4-finger devices.

IV. RESULTS AND DISCUSSION

To optimize the layout design and to investigate the impact of raising gate stem on noise performance, AlGaN/GaN HEMTs with different gate peripheries and with different heights of gate stems were fabricated and evaluated in this study. In this section, transfer characteristics of the devices are provided at first. Afterward, the noise characteristics of NF_{min} and the associated gain (G_{asso}) will be displayed. Then, the S-parameters and extracted values of parameters will be shown to explain the trends of the measured NF_{min}. Finally, the large-signal power characteristics of the devices will be displayed.

A. IMPACT OF DIFFERENT GATE PERIPHERIES ON NOISE AND POWER PERFORMANCE OF ALGAN/GAN HEMTS

To optimize the device layout for best noise performance, AlGaN/GaN HEMTs, whose gate stem heights are 150 nm, with 4 types of gate peripheries (2×25/4×25/2×50/4×50 um) were prepared. A device with a wider channel width is expected to have a lower source resistance (R_S) value but larger capacitance such as C_{gs} and C_{gd}, while one with more gate fingers in parallel tends to have reduced gate resistance (R_G) value. On the other hand, varying the gate periphery also involves the changes the intrinsic transconductance (g_m) and output conductance (g_o), which are also critical to determine NF_{min} according to Equation (1). Therefore, it is important to investigate the change in these parameters when finding out the optimal gate periphery.

Fig. 5 shows the transfer characteristics of the devices with different gate peripheries, which were conducted under 10 V drain bias voltage (V_{DS}). The measured steady-state current densities (I_{DSS}) and the maximum transconductances ($G_{m,max}$) are summarized in Table 1. There is no significant difference in the transfer curves or $G_{m,max}$ for various gate peripheries.

Next, the noise characteristics were measured from 18 to 40 GHz under $V_{DS} = 10$ V and gate voltage (V_{GS}) biased for current density (I_{DS}) equals 25% of I_{DSS}. NF_{min} and G_{asso} of the devices with respect to frequency are shown in Fig. 6, and their values at 28 GHz are summarized in Table 2. The measured results show the 4×50um device owns the lowest

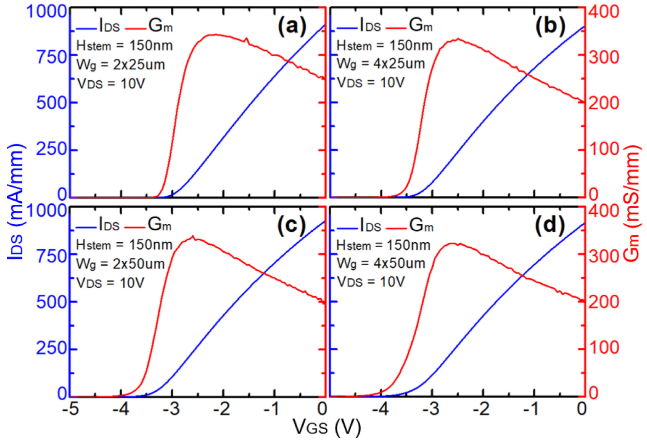

FIGURE 5. IDVG curves of AlGaN/GaN HEMTs with gate width (W_g) of (a) 2×25 um (b) 4×25 um (c) 2×50 um and (d) 4×50 um.

TABLE 1. Transfer characteristics of AlGaN/GaNs with different gate peripheries.

W_g	2x25um	4x25um	2x50um	4x50um
I_{DSS} (mA/mm)	912	904	926	915
$G_{m,max}$ (mS/mm)	342	332	334	322

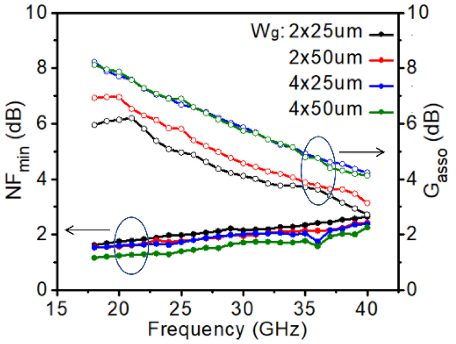

FIGURE 6. NF_{min} and G_{asso} of AlGaN/GaN HEMTs with different gate peripheries as a function of frequency.

TABLE 2. NF_{min} and G_{asso} at 28 GHz of AlGaN/GaN HEMTs with different gate peripheries.

W_g	2x25um	4x25um	2x50um	4x50um
NF_{min} @28GHz	2.12dB	1.93dB	1.89dB	1.51dB
G_{asso} @28GHz	4.37dB	6.21dB	4.98dB	6.15dB

NF_{min} with the level of G_{asso} as high as the 4×25um device, while the 2×25um device has the greatest NF_{min} and lowest G_{asso} characteristics. On the other hand, the devices with same gate periphery (4×25um and 2×50um) own similar characteristic of NF_{min}.

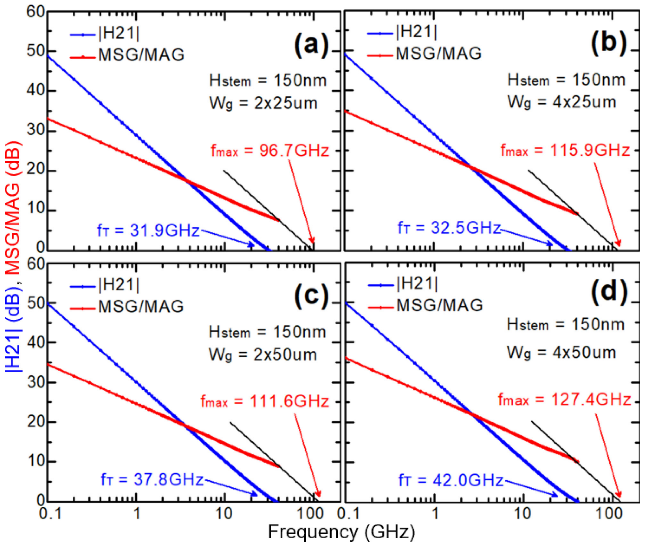

FIGURE 7. Measured |H21| and MSG/MAG of AlGaN/GaN HEMTs with gate width of (a) 2×25 um (b) 4×25 um (c) 2×50 um and (d) 4×50 um.

TABLE 3. Extracted values of elements of AlGaN/GaN HEMTs with different gate peripheries.

W_g	2x25um	4x25um	2x50um	4x50um
C_{gs}	60.5fF	110.6fF	94.8fF	176.3fF
C_{gd}	10.8fF	18.8fF	16.3fF	26.7fF
R_S	8.9Ω	5.5Ω	5.4Ω	3.2Ω
R_G	6.8Ω	3.6Ω	7.1Ω	3.8Ω
R_D	13.6Ω	8.5Ω	8.4Ω	5.5Ω
g_m	20.5mS	40.5mS	41.1mS	82.9mS
g_o	0.6mS	1.1mS	1.0mS	2.1mS
Δ	1973.2fF·Ω	1939.7fF·Ω	1945.2fF·Ω	1865.4fF·Ω

The S-parameters were measured using same bias voltages as the noise measurement. Fig. 7 (a) to (d) show the |H21| gain and MSG/MAG of the devices, and the estimated values of cut-off frequency (f_T) and maximum oscillation frequency (f_{max}) are labelled. The formulas of f_T and f_{max} can be expressed as Equations (2) and (3) below [25], [26]:

$$f_T = \frac{\frac{g_m}{2\pi}}{(C_{gs}+C_{gd})\times\left[1+(R_S+R_D)g_o\right]+g_m C_{gd}(R_S+R_D)} \tag{2}$$

$$f_{\max} = \frac{f_T}{2\sqrt{g_o(R_G+R_S)+2f_T C_{gd} R_G}} \tag{3}$$

Based on the measured S-parameters, the values of parameters involved in f_T, f_{max}, and Fukui's equation are extracted by cold-FET method and then summarized in Table 3. It is obtained that device with wider gate periphery owns a lower source resistance (R_S) value with increased C_{gs} and C_{gd}, and 4-finger devices have reduced R_G values compared with 2-finger ones; moreover, g_m and g_o almost have proportional relationship with the gate periphery. For 4×25um and 2×50um devices with the same gate periphery, the 4×25um device owns slightly greater C_{gs} and C_{gd}, which may result from a more significant fringing effect of using more fingers, and reduced R_G due to more fingers in parallel, leading to its inferior f_T but superior f_{max} values and so do the similar NF_{min} characteristics. Then by substituting the values

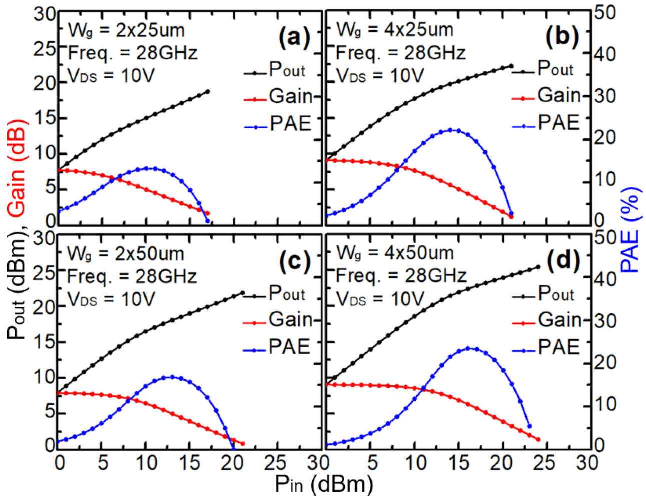

FIGURE 8. Large-signal power performance at 28 GHz of AlGaN/GaN HEMTs with gate width of (a) 2×25 um (b) 4×25 um (c) 2×50 um and (d) 4×50 um.

TABLE 4. Large-signal power characteristics at 28 GHz of AlGaN/GaN HEMTs with different gate peripheries.

W_g	2x25um	4x25um	2x50um	4x50um
OP_{1dB}	0.37W/mm	0.51W/mm	0.39W/mm	0.61W/mm
$P_{out,max}$	1.49W/mm	1.67W/mm	1.54W/mm	1.75W/mm
G_p	7.84dB	9.13dB	7.95dB	9.08dB
PAE_{max}	13.3%	22.2%	16.9%	23.5%
MSG/MAG @28GHz	9.01dB	10.73dB	10.33dB	11.90dB

of extracted parameters into Fukui equation, the trends of NF_{min} can be examined. A symbol Δ is used to represent the contribution of extracted parameters to NF_{min} as:

$$\Delta = \left(C_{gs} + C_{gd}\right)\sqrt{\frac{R_G + R_S}{g_m}} \tag{4}$$

According to the quantitative results, the 4×50um device with the widest gate periphery is estimated to achieve the lowest NF_{min}, while the 2×25um device may tend to own the greatest NF_{min}. Unlike g_m, the capacitance does not proportionally increase as the gate periphery becomes wider. NF_{min} is thereby benefited from a wider gate periphery before the increment in $C_{gs}+C_{gd}$ exceeds root of g_m.

The load-pull measurements at 28 GHz are shown in Fig. 8. Note the V_{GS} was set at class AB mode and V_{DS} was 10 V, like the bias conditions for the noise measurements. The impedances of both the source port and load port were tuned for the maximum output power of the devices. The large-signal power characteristics of devices and their MSG/MAG values at 28 GHz are summarized in Table 4. The focused device with 4×50um gate periphery again owns superior power characteristics, which may result from the highest MSG/MAG at 28 GHz. It achieved output power density at 1 dB compression (OP_{1dB}) of 0.61 W/mm, linear power gain (G_p) of 9.08 dB, and power-added efficiency (PAE) of 23.5% at 28 GHz. Because of its superior noise and power performance, the layout of 4×50um device was picked for further explore possible effects of gate stem heights.

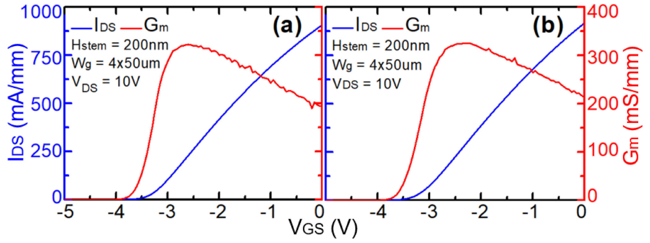

FIGURE 9. IDVG curves of AlGaN/GaN HEMTs with gate stem height (H_{stem}) of (a) 200 nm and (b) 250 nm.

TABLE 5. Transfer characteristics of AlGaN/GaN HEMTs with different gate stem heights.

H_{stem}		150nm	200nm	250nm
I_{DSS}	(mA/mm)	915	906	916
$G_{m,max}$	(mS/mm)	322	322	324

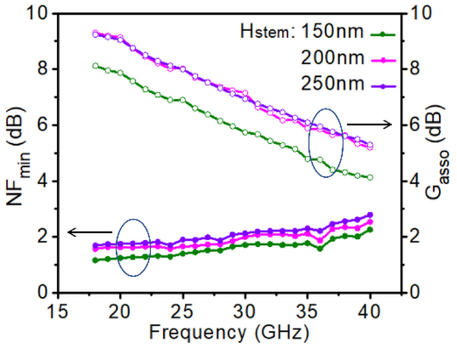

FIGURE 10. Minimum noise figure and associated gain of devices with different gate stem heights as a function of frequency.

B. IMPACT OF DIFFERENT GATE STEM HEIGHTS ON NOISE AND POWER PERFORMANCE OF ALGAN/GAN HEMTS

AlGaN/GaN HEMTs with properly raised Γ-shaped gate has proven to have lower parasitic capacitance and thus better power performance for its tall stem structure [24]; however, it may lead to greater R_G. According to Equation (1), NF_{min} is positively correlated not only to $C_{gs}+C_{gd}$ but also to the square root of R_g+R_s. Therefore, the tall gate stem structure may weigh on the noise behaviors, as will be further discuss later. In this discussion, AlGaN/GaN HEMTs, whose gate widths are 4×50 um, with different heights of gate stems (150/200/250 nm) were prepared.

The transfer characteristics of the devices with stem heights 200 and 250 nm are shown in Fig. 9 in reference to what is shown for the 150 nm stem shown in Fig. 5(d). Their I_{DSS} and $G_{m,max}$ values are summarized in Table 5 for convenience of comparison. Apparently, the gate stem height has no significant effects on the DC performance.

TABLE 6. NF_{min} and G_{asso} at 28 GHz of AlGaN/GaN HEMTs with different gate stem heights.

H_{stem}	150nm	200nm	250nm
NF_{min} @28GHz	1.51dB	1.73dB	1.87dB
G_{asso} @28GHz	6.15dB	7.37dB	7.32dB

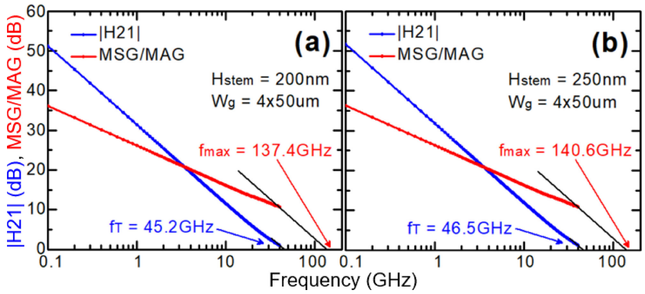

FIGURE 11. Measured |H21| and MSG/MAG of AlGaN/GaN HEMTs with gate stem height of (a) 200 nm and (b) 250 nm.

TABLE 7. Extracted values of parasitic elements of 4×50um AlGaN/GaN HEMTs with different stem heights.

H_{stem}	150nm	200nm	250nm
C_{gs}	176.3fF	171.9fF	169.5fF
C_{gd}	26.7fF	20.1fF	17.1fF
R_S	3.2Ω	3.3Ω	3.3Ω
R_G	3.8Ω	5.0Ω	5.6Ω
R_D	5.5Ω	5.3Ω	5.4Ω
g_m	82.9mS	83.2mS	83.1mS
g_o	2.1mS	2.1mS	2.1mS
Δ	1865.4fF·Ω	1917.7fF·Ω	1931.1fF·Ω

Their noise characteristics were also measured from 18 to 40 GHz under $V_{DS} = 10$ V and gate voltage (V_{GS}) biased for current density (I_{DS}) equals 25% of I_{DSS}. Fig. 10 shows the NF_{min} and G_{asso} characteristics with respect to frequency, and their values at 28 GHz are summarized in Table 6. It is observed that the level of NF_{min} becomes higher as the stem height increases, and there is no obvious difference between associated gains of 200nm-stem and 250nm-stem devices.

The S-parameters were measured using same bias voltages as the noise measurement as well. Fig. 11 shows the |H21| gain and MSG/MAG of 200nm-stem and 250nm-stem devices in reference to what is shown for the 150 nm stem shown in Fig. 7(d). The estimated f_T/f_{max} values of the 200nm-stem device (45.2/137.4 GHz) and the 250nm-stem device (46.5/140.6 GHz) are much better than the 150nm-stem device (42.0/127.4 GHz) due to the reduction in C_{gs} and C_{gd}. Again, the values of parameters involved in f_T, f_{max}, and Fukui's equation are extracted and summarized in Table 7. It is obtained that as the height of stem increases, C_{gs} and C_{gd} reduces but R_g greatly increases. According to results of Δ, a taller gate stem leads to the greatly increase in gate resistance, making the increment of the square root of R_G+R_S exceeds the reduction in $C_{gs}+C_{gd}$. Therefore, even though the tall gate stem structure improves the parasitic capacitance of a device, NF_{min} still degrades.

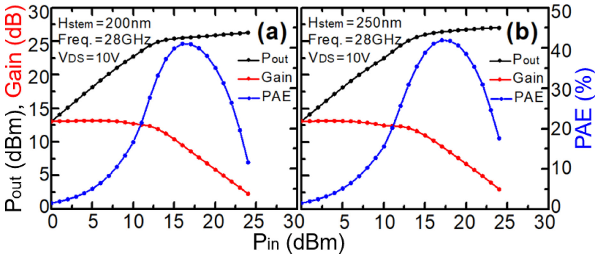

FIGURE 12. Large-signal power performance at 28 GHz of AlGaN/GaN HEMTs with gate stem height of (a) 200 nm and (b) 250 nm.

TABLE 8. Large-signal power characteristics at 28 GHz of devices with different gate stem heights.

H_{stem}	150nm	200nm	250nm
OP_{1dB}	0.61W/mm	1.55W/mm	1.62W/mm
$P_{out,max}$	1.75W/mm	2.13W/mm	2.50W/mm
G_p	9.08dB	13.18dB	13.16dB
PAE_{max}	23.5%	41.1%	42.0%
MSG/MAG @28GHz	11.90dB	12.18dB	12.32dB

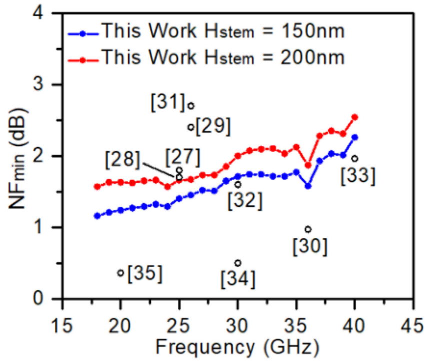

FIGURE 13. Comparison of the minimum noise figure of GaN devices at Ka-band.

The load-pull measurements at 28 GHz for the stem heights of 200 and 250 nm devices are shown in Fig. 12 for comparison with what has been shown in Fig. 8 (d) for their 150 nm counterpart. Note the V_{GS} was also set at class AB mode with $V_{DS} = 10$ V. The large-signal power characteristics of the devices and their MSG/MAG values at 28 GHz are summarized in Table 8. According to the results, the power characteristics of the 200nm-stem and 250nm-stem devices are similar and are far superior to the 150nm-stem counterpart. At 28 GHz, the 200nm-stem device achieves OP_{1dB} of 1.55 W/mm, $P_{out,max}$ of 2.13 W/mm, G_p of 13.18 dB, and PAE of 41.1%. Thus, all things considered, with outstanding power performance and adequate noise performance, the device with H_{stem} of 200 nm stands out as a competitive possibility for both LNA and PA millimeter-wave applications.

In this spirit, Table 9 and Fig. 13 compare the noise and RF power performances of the 150nm and 200nm devices

TABLE 9. Comparison of noise and power performances of GaN devices at Ka-band.

	Noise Performance				Large-Signal Power Performance				
	Freq.	V_{DS}	NF_{min}	G_{asso}	Freq.	V_{DS}	$P_{out,max}$	G_p	PAE_{max}
This work H_{stem}=200nm	28GHz	10V	1.73dB	7.37dB	28GHz	10V	2.13W/mm	13.18dB	41.1%
This work H_{stem}=150nm	28GHz	10V	1.51dB	6.15dB	28GHz	10V	1.75W/mm	9.08dB	23.5%
[27]	25GHz	6V	~1.8dB	~8.5dB	30GHz	20V	2.5W/mm	~8.0dB	25%
[28]	25GHz	5V	~1.7dB	~11.0dB	14GHz	15V	2.1W/mm	14.5dB	36.0%
[29]	26GHz	5V	~2.4dB	~7.0dB	-	-	-	-	-
[30]	36GHz	5V	0.97dB	7.5dB	-	-	-	-	-
[31]	26GHz	16V	~2.7dB	~5.5dB	-	-	-	-	-
[32]	30GHz	10V	1.6dB	5.0dB	-	-	-	-	-
[33]	40GHz	5V	1.96dB	7.29dB	-	-	-	-	-
[34]	30GHz	5V	0.5dB	13.5dB	-	-	-	-	-
[35]	20GHz	2V	0.36dB	16.5dB	-	-	-	-	-

from this work with the data in the Ka-band reported in literature. In all, the AlGaN/GaN HEMT with $H_{stem} = 200$ nm turns out to compete well with peers for both LNA and PA applications in Ka-band.

V. CONCLUSION

The impacts of layout designs with different gate peripheries and heights of gate stems on the noise performance of the Γ-gate AlGaN/GaN HEMTs were investigated. Among the devices with different gate peripheries, the 4×50um device owns best measured noise performance: minimum noise figure of 1.5 dB and associated gain of 6.2 dB at 28 GHz. The raised gate stem structure is applied to alleviate the parasitic capacitances and to enhance the RF power performance; however, it increases the gate resistance. As the stem height increases, even though the capacitance is reduced, the minimum noise figure becomes higher due to the great increment in gate resistance. Based on the experiment results, the 200nm-stem device maintains competitiveness in noise and RF power performance at Ka-band, and thus can be applied for LNA and PA integration as a single chip solution for the RF circuit design.

REFERENCES

[1] H.-Y. Chang, Y.-C. Liu, S.-H. Weng, C.-H. Lin, Y.-L. Yeh, and Y.-C. Wang, “Design and analysis of a DC–43.5-GHz fully integrated distributed amplifier using GaAs HEMT–HBT cascode gain stage,” *IEEE Trans. Microw. Theory Techn.*, vol. 59, no. 2, pp. 443–455, Feb. 2011.

[2] K. Elgaid, H. McLelland, M. Holland, D. A. J. Moran, C. R. Stanley, and I. G. Thayne, “50-nm T-gate metamorphic GaAs HEMTs with fT of 440 GHz and noise figure of 0.7 dB at 26 GHz,” *IEEE Electron Device Lett.*, vol. 26, no. 11, pp. 784–786, Nov. 2005.

[3] A. Leuther et al., “70 nm low-noise metamorphic HEMT technology on 4 inch GaAs wafers,” in *Proc. Int. Conf. Indium Phosphide Relat. Mater.*, Santa Barbara, CA, USA, 2003, pp. 215–218.

[4] C. S. Whelan et al., “Millimeter-wave low-noise and high-power metamorphic HEMT amplifiers and devices on GaAs substrates,” *IEEE J. Solid-State Circuits*, vol. 35, no. 9, pp. 1307–1311, Sep. 2000.

[5] C. Wang et al., “Effect of the indium compositions in tri-gate InxGa1-xAs HEMTs for high-frequency low noise application,” *ECS J. Solid State Sci. Technol.*, vol. 11, no. 11, Nov. 2022, Art. no. 115006.

[6] T. Kikkawa et al., “High performance and high reliability AlGaN/GaN HEMTs,” *Phys. Status Solidi A*, vol. 206, no. 6, pp. 1135–1144, 2009.

[7] U. K. Mishra, P. Parikh, and Y.-F. Wu, “AlGaN/GaN HEMTs-an overview of device operation and applications,” *Proc. IEEE*, vol. 90, no. 6, pp. 1022–1031, Jun. 2002.

[8] R. Vetury, N. Zhang, S. Keller, and U. K. Mishra, “The impact of surface states on the DC and RF characteristics of AlGaN/GaN HFETs,” *IEEE Trans. Electron Devices*, vol. 48, no. 3, pp. 560–566, Mar. 2001.

[9] S. T. Sheppard et al., “High-power microwave GaN/AlGaN HEMTs on semi-insulating silicon carbide substrates,” *IEEE Electron Device Lett.*, vol. 20, no. 4, pp. 161–163, Apr. 1999.

[10] Y. C. Lin et al., “Gallium nitride (GaN) high-electron-mobility transistors with thick copper metallization featuring a power density of 8.2 W/mm for ka-band applications,” *Micromachines*, vol. 11, no. 2, p. 222, Feb. 2020.

[11] S. Colangeli, A. Bentini, W. Ciccognani, E. Limiti, and A. Nanni, “GaN-based robust low-noise amplifiers,” *IEEE Trans. Electron Devices*, vol. 60, no. 10, pp. 3238–3248, Oct. 2013.

[12] M. Chen et al., “A 1–25 GHz GaN HEMT MMIC low-noise amplifier,” *IEEE Microw. Compon. Lett.*, vol. 20, no. 10, pp. 563–565, Oct. 2010.

[13] M. Rudolph, “GaN HEMTs for low-noise amplification—status and challenges,” in *Proc. Integr. Nonlinear Microw. Millimetre-Wave Circuits Workshop (INMMiC)*, Graz, Austria, 2017, pp. 1–4.

[14] S. Lardizabal, K. C. Hwang, J. Kotce, A. Brown, and A. Fung, “Wideband W-band GAN LNA MMIC with state-of-the-art noise figure,” in *Proc. IEEE Compound Semicond. Integr. Circuit Symp. (CSICS)*, Austin, TX, USA, 2016, pp. 1–4, doi: 10.1109/CSICS.2016.7751079..

[15] I. Kallfass et al., “A highly linear 84 GHz low noise amplifier MMIC in AlGaN/GaN HEMT technology,” in *Proc. IEEE MTT-S Int. Microw. Workshop Series Millimeter Wave Integr. Technol.*, Sitges, Spain, 2011, pp. 144–147.

[16] M. Micovic et al., “Ka-band LNA MMIC’s realized in Fmax >580 GHz GaN HEMT technology,” in *Proc. IEEE Compound Semicond. Integr. Circuit Symp. (CSICS)*, Austin, TX, USA, 2016, pp. 1–4.

[17] A. Jarndal and G. Kompa, “A new small-signal modeling approach applied to GaN devices,” *IEEE Trans. Microw. Theory Techn.*, vol. 53, no. 11, pp. 3440–3448, Nov. 2005.

[18] H. Fukui, “Optimal noise figure of microwave GaAs MESFET’s,” *IEEE Trans. Electron Devices*, vol. 26, no. 7, pp. 1032–1037, Jul. 1979.

[19] Z. H. Liu, G. I. Ng, and S. Arulkumaran, “Analytical modeling of high-frequency noise including temperature effects in GaN HEMTs on high-resistivity Si substrates,” *IEEE Trans. Electron Devices*, vol. 57, no. 7, pp. 1485–1491, Jul. 2010.

[20] T. Takahashi, K. Makiyama, N. Hara, M. Sato, and T. Hirose, "Improvement in high frequency and noise characteristics of InP-based HEMTs by reducing parasitic capacitance," in *Proc. 20th Int. Conf. Indium Phosphide Relat. Mater.*, Versailles, France, 2008, pp. 1–4.

[21] C. Andrei, R. Doerner, S. A. Chevtchenko, W. Heinrich, and M. Rudolph, "On the optimization of GaN HEMT layout for highly rugged low-noise amplifier design," in *Proc. 12th Eur. Microw. Integr. Circuits Conf. (EuMIC)*, Nuremberg, Germany, 2017, pp. 244–247.

[22] M. Roy, D. George, and S. Bhaumik, "Study of dependence of HEMT noise parameters on gate periphery in microwave LNA design," in *Proc. 7th Eur. Microw. Integr. Circuits Conf.*, 2012, pp. 389–392.

[23] J. Gao, C. L. Law, H. Wang, S. Aditya, and G. Boeck, "A new method for pHEMT noise-parameter determination based on 50-Ω noise measurement system," *IEEE Trans. Microw. Theory Techn.*, vol. 51, no. 10, pp. 2079–2089, Oct. 2003.

[24] P.-H. Lee et al., "A tall gate stem GaN HEMT with improved power density and efficiency at ka-band," *IEEE J. Electron Devices Soc.*, vol. 11, pp. 36–42, 2023.

[25] L.-C. Chang, K.-C. Hsu, Y.-T. Ho, W.-C. Tzeng, Y.-L. Ho, and C.-H. Wu, "High f_{max} × LG Product of AlGaN/GaN HEMTs on silicon with thick rectangular gate," *IEEE J. Electron Devices Soc.*, vol. 8, pp. 481–484, 2020.

[26] S. Bouzid-Driad et al., "AlGaN/GaN HEMTs on silicon substrate with 206-GHz FMAX," *IEEE Electron Device Lett.*, vol. 34, no. 1, pp. 36–38, Jan. 2013.

[27] S. Piotrowicz et al., "12W/mm with 0.15μm InAlN/GaN HEMTs on SiC technology for K and Ka-bands applications," in *Proc. IEEE MTT-S Int. Microw. Symp. (IMS)*, Tampa, FL, USA, 2014, pp. 1–3.

[28] Y. Murase, K. Asano, I. Takenaka, Y. Ando, H. Takahashi, and C. Sasaoka, "T-Shaped Gate GaN HFETs on Si with improved breakdown voltage and f_{MAX}," *IEEE Electron Device Lett.*, vol. 35, no. 5, pp. 524–526, May 2014.

[29] S. D. Nsele, L. Escotte, J.-G. Tartarin, and S. Piotrowicz, "Noise characteristics of AlInN/GaN HEMTs at microwave frequencies," in *Proc. 22nd Int. Conf. Noise Fluctuat. (ICNF)*, Montpellier, France, 2013, pp. 1–4.

[30] F. Medjdoub et al., "Sub-1-dB minimum-noise-figure performance of GaN-on-Si transistors up to 40 GHz," *IEEE Electron Device Lett.*, vol. 33, no. 9, pp. 1258–1260, Sep. 2012.

[31] T. Huang, O. Axelsson, T. N. T. Do, M. Thorsell, D. Kuylenstierna, and N. Rorsman, "Influence on noise performance of GaN HEMTs with in situ and low-pressure-chemical-vapor-deposition SiNx passivation," *IEEE Trans. Electron Devices*, vol. 63, no. 10, pp. 3887–3892, Oct. 2016.

[32] C.-T. Chang et al., "30-GHz low-noise performance of 100-nm-gate-recessed n-GaN/AlGaN/GaN HEMTs," *IEEE Electron Device Lett.*, vol. 31, no. 2, pp. 105–107, Feb. 2010.

[33] Y.-K. Lin et al., "AlGaN/GaN HEMTs with damage-free neutral beam etched gate recess for high-performance millimeter-wave applications," *IEEE Electron Device Lett.*, vol. 37, no. 11, pp. 1395–1398, Nov. 2016.

[34] J.-S. Moon et al., "360 GHz f_{MAX} graded-channel AlGaN/GaN HEMTs for mmW low-noise applications," *IEEE Electron Device Lett.*, vol. 41, no. 8, pp. 1173–1176, Aug. 2020.

[35] K. Shinohara et al., "Scaling of GaN HEMTs and schottky diodes for submillimeter-wave MMIC applications," *IEEE Trans. Electron Devices*, vol. 60, no. 10, pp. 2982–2996, Oct. 2013.